A new family of metal borohydride ammonia borane complexes: Synthesis, structures, and hydrogen storage properties†

Hui Wu,*[ab] Wei Zhou,[ab] Frederick E. Pinkerton,[c] Martin S. Meyer,[c] Gadipelli Srinivas,[ad] Taner Yildirim,[ad] Terrence J. Udovic[a] and John J. Rush[ab]

Received 20th May 2010, Accepted 28th May 2010
DOI: 10.1039/c0jm01542c

We report the first two examples of borohydride ammonia borane complexes: $Li_2(BH_4)_2NH_3BH_3$ and $Ca(BH_4)_2(NH_3BH_3)_2$. Their structures are successfully determined using a combination of X-ray diffraction and first-principles calculations. Both structures are composed of alternating layers of borohydride and ammonia borane. Examination of bond lengths indicates that this arrangement is stabilized *via* dihydrogen bonding between ammonia borane and their surrounding BH_4^-, and the interactions between ammonia borane ligands and cations. Our experimental results show that more than 10 wt% and 11 wt% hydrogen can be released from $Li_2(BH_4)_2NH_3BH_3$ and $Ca(BH_4)_2(NH_3BH_3)_2$, respectively. Negligible ammonia was detected compared to ammonia borane and its ammidoborane derivatives. Further improvements are needed to reduce borazine emission. Cycling studies show that decomposed $Li_2(BH_4)_2NH_3BH_3$ and $Ca(BH_4)_2(NH_3BH_3)_2$ can be partially hydrogenated under hydrogen pressures at high temperatures.

1 Introduction

Extensive efforts have been focused on boron-containing hydrogenous materials primarily due to the light constitutional boron element and the resulting high hydrogen storage capacities. Among them, ammonia borane (NH_3BH_3, AB) has attracted great interest due to its combined low molecular weight (30.7 g/mol) and high gravimetric hydrogen capacity. NH_3BH_3 contains both hydridic B–H and protic N–H bonds and a strong enough B–N bond that hydrogen release from solid AB is favored over dissociation to ammonia and diborane under noncatalytic conditions.[1] Many approaches have been developed to understand and control the properties of AB to be practical in terms of reduced dehydrogenation temperatures,[2] accelerated H_2 release kinetics,[2–7] and/or minimized borazine release.[4] However, there is no single approach that can achieve all these improvements. One avenue for modifying AB in this regard has been to form metal amidoboranes, *e.g.*, $LiNH_2BH_3$, $NaNH_2BH_3$, and $Ca(NH_2BH_3)_2$, which have been reported to exhibit intriguing and advantageous properties over AB as potential hydrogen storage materials.[8–11] Continuous efforts have been made to explore the related materials *via* mixing amides such as $LiNH_2$[12] and $Ca(NH_2)_2$[13] with AB. The former combination led to an amorphous phase, while the latter formed a crystalline amidoborane ammoniate $Ca(NH_2BH_3)\cdot 2NH_3$.

Herein, we report the syntheses and detailed structural and property characterization of two new boron-containing hydride materials *via* the combination of AB and the light weight borohydrides, $LiBH_4$ and $Ca(BH_4)_2$, aimed at exploring new high H content compounds with potential applications for hydrogen storage. Introducing borohydrides is desired to improve the purity of gaseous dehydrogenation products, as ammonia was reported as an undesirable dehydrogenation product of the metal amidoboranes,[14] and the $LiNH_2$-AB and $Ca(NH_2)_2$-AB systems.[13] $LiBH_4$ is a complex hydride that has received close attention due to its high gravimetric and volumetric hydrogen storage capacities (13.6 wt % and 0.092 kg/L). Many efforts have been made to improve the thermodynamics, hydrogen exchange kinetics and cycling properties of $LiBH_4$, including destabilization by additives,[15,16] and tuning particle size.[17] $Ca(BH_4)_2$ can be heated to 400 °C to release 9.6 wt% hydrogen.[18] Upon addition of catalytic amounts of the dopants, $TiCl_3$ and Pd, $Ca(BH_4)_2$ can be rehydrogenated at 700 bar and 400–440 °C with a 60% yield. Through a combination of these borohydrides and ammonia borane, the two new crystalline compounds, $Li_2(BH_4)_2NH_3BH_3$ and $Ca(BH_4)_2(NH_3BH_3)_2$, were formed. These materials possess completely novel structures with attractive hydrogen contents. Our findings are useful as a guideline and inspiration for the design and synthesis of other as of yet undiscovered complex hydrides for hydrogen storage.

2 Experimental section

Lithium borohydride ammonia borane $Li_2(BH_4)_2NH_3BH_3$ (LiBH · AB for short) and calcium borohydride ammonia borane $Ca(BH_4)_2(NH_3BH_3)_2$ (CaBH · AB for short) were prepared by ball milling the stoichiometric ratios of either $LiBH_4$ (95%, Aldrich)[19] or $Ca(BH_4)_2$ (Aldrich) with NH_3BH_3 (90%,

[a]*NIST Center for Neutron Research, National Institute of Standards and Technology, Gaithersburg, MD, 20899-6102, USA. E-mail: huiwu@nist.gov; Fax: +1-301-921-9847; Tel: +1-301-975-2387*
[b]*Department of Materials Science and Engineering, University of Maryland, College Park, MD, 20742-2115, USA*
[c]*Chemical Sciences and Materials Systems Laboratory, General Motors Research and Development Center, Warren, MI, 48090-9055, USA*
[d]*Department of Materials Science and Engineering, University of Pennsylvania, Philadelphia, PA, 19104-6272, USA*

† Electronic supplementary information (ESI) available: Tables of structure solutions, atomic coordinates and bond lengths for $Li_2(BH_4)_2NH_3BH_3$ and $Ca(BH_4)_2(NH_3BH_3)_2$. Refined XRD patterns. Additional structure figures. Cycling studies of LiBH · AB and CaBH · AB. See DOI: 10.1039/c0jm01542c

Aldrich) powders under 1 bar He. The $LiBH_4$-NH_3BH_3 and $Ca(BH_4)_2$-NH_3BH_3 powder mixtures were milled using a Fritsch Pulverisette 7 planetary mill at 250 rpm for 2 h and 300 rpm for 3 h. After milling, the mixtures were stored in a He-filled glovebox for further structural and property characterizations. All sample handling was performed in the He-filled glovebox due to the air-sensitivity of these complex hydrides.

Phase identification and equilibrium were monitored on samples sealed in 0.7 mm glass capillaries using a Rigaku X-ray diffractometer with a Cu K_α source. Data for structural studies were collected over 24 h at room temperature in the 2θ range of 5–70° with a step size of 0.02°. Rietveld structural refinements were done using the GSAS package.[20]

Neutron vibrational spectra (NVS) were measured at 5 K using the BT-4 Filter-Analyzer Neutron Spectrometer (FANS) with the Cu(220) monochromator under conditions that provided energy resolutions of 2–4.5% over the vibrational energy range probed.

Dehydrogenation of $Li_2(BH_4)_2NH_3BH_3$ and $Ca(BH_4)_2$-$(NH_3BH_3)_2$ was characterized by temperature-programmed-desorption (TPD) performed on a Sieverts-type apparatus described previously.[21] Samples were heated to 450 °C at 2 °C/min. Rehydrogenation of the desorbed samples was conducted using the same apparatus under 50 bar H_2 at 150 °C and 300 °C, respectively. After absorption, samples were cooled to room temperature, and the remaining H_2 was purged under dynamic vacuum. A second desorption was conducted using the same conditions as the first desorption run.

Weight loss and semi-quantitative mass spectrometry (MS) measurements were conducted in a Cahn TG-2151 high pressure thermogravimetric analyzer (TGA). Approximately 200 mg of sample were loaded into a stainless steel bucket and transferred into the TGA under a cover of liquid pentane to protect the sample from air exposure during transfer and purging. The pentane evaporated while the TGA was purged with flowing He gas. After evaporation the sample was heated at 5 °C/min to 450 °C in flowing He gas at 1.3 bar. The exhaust gas was sampled by an SRS CIS 100 MS operated in residual gas analysis (RGA) mode. Based on species identified in an initial survey that sampled all mass channels from 6 to 199 amu, the RGA monitored the partial pressures for H_2 (2 amu), He (4 amu), CH_4 (16 amu), NH_3 (17 amu), H_2O (18 amu), B_2H_6 (24 amu), C_2H_4 (27 amu), N_2/CO (28 amu), O_2 (32 amu), and $(BH)_3(NH)_3$ (80 amu); for diborane and ethylene a secondary crack of the mass fraction pattern was used to distinguish these from other gases with an overlapping cracking pattern. Gas concentrations were referenced to the He cover gas and the cracking pattern of each species was taken into account in extracting semi-quantitative information. The MS was calibrated for common gases including He, H_2, N_2, O_2, H_2O, NH_3, CH_4, and diborane B_2H_6, providing semi-quantitative measurements (±20% relative) of the contributions of these gases to the weight loss. The amount of borazine (s-triazaborane) $(BH)_3(NH)_3$ and ethylene (C_2H_4) were not calibrated.

Rehydrogenation of the desorbed sample was also conducted in the high pressure TGA using flowing H_2 gas at 82 bar. The temperature was increased from room temperature in steps of 50 °C up to 400 °C. The MS was not used during hydrogenation. After absorption, the sample was cooled to room temperature, the H_2 pressure was decreased to 1.3 bar, and the remaining H_2 was purged from the TGA with flowing He. A second desorption run was conducted under the same conditions as the original. Finally, a second absorption was conducted and the absorbed product was extracted from the TGA using a sealed plastic bag purged with He.

First-principles calculations based on density-functional theory (DFT) were performed by using the PWSCF package.[22] We used a Vanderbilt-type ultrasoft potential with Perdew–Burke–Ernzerhof exchange correlation. A cutoff energy of 544 eV was found to be enough for the total energy to converge within 0.5 meV/atom. Car–Parrinello molecular dynamics simulations[23] were used to help in searching for the most likely crystal structures. The conventional unit cells were used, with the cell dimensions fixed at the experimental values. The initial system temperature was set to 600 K. The system was first allowed to evolve and equilibrate for 20 ps, and then the system temperature was slowly decreased to 0 K in a period of 20 ps. Structure optimizations on the resulting candidate structures at 0 K were further performed with respect to atomic positions, with the lattice parameters fixed at the experimental values. Lattice dynamics calculations were then performed on the relaxed structures using the supercell method with finite displacements,[24] to rule out unstable candidates. A 2 × 2 × 1 supercell was used for LiBH · AB, and a 2 × 2 × 2 supercell was used for CaBH · AB. The total energies of the stable candidate structures at 0 K, including corrections for the zero-point motion, were also evaluated. This information was used in combination with XRD pattern matching to derive the best crystal structure solutions of the borohydride ammonia borane compounds.

3 Results and discussion

3.1 Crystal structure of $Li_2(BH_4)_2(NH_3BH_3)$ and $Ca(BH_4)_2(NH_3BH_3)_2$

The XRD reflections of the ball milled $LiBH_4/NH_3BH_3$ mixtures can be indexed using an orthorhombic *Pnma* cell (No. 62) with $a = 8.3118(8)$Å, $b = 12.428(1)$ Å and $c = 6.5944(7)$ Å, and those of the $Ca(BH_4)_2/NH_3BH_3$ mixtures can be indexed by the orthorhombic *Aba*2 (No.41) cell with $a = 8.265(1)$ Å, $b = 13.478(2)$ Å, and $c = 8.136(1)$ Å. With the indexed lattice parameters, the crystal structures of the lithium and calcium borohydride ammonia borane were then solved using the combined direct methods and first-principles molecular dynamics simulated annealing. While the quality and insensitivity of XRD do not allow accurate determination of atomic positions (particularly for lightweight Li and H), with the help of molecular dynamics simulations, we were able to derive the most likely crystal structure solutions with favorable BH_4^- and NH_3BH_3 orientations. Rietveld structural refinements for both compounds were then performed using these structure models. It can be seen from inspection of the XRD data refinement that all the diffraction peaks of LiBH · AB and CaBH · AB can be very well fitted using the determined structure models (Figure S1 and S2 in the Supporting Information) with agreement factors of $R_{wp} = 0.0562$, $R_p = 0.0435$ for LiBH · AB and $R_{wp} = 0.0607$, $R_p = 0.0524$ for CaBH · AB, which strongly

supports the validity of our structure solutions. The detailed structural information is given in the Supporting Information. More accurate structural details can be easily obtained by refining neutron diffraction data on ^{11}B-isotope enriched samples in the future.

The fully relaxed crystal structures for $Li_2(BH_4)_2NH_3BH_3$ and $Ca(BH_4)_2(NH_3BH_3)_2$ from the first-principles calculations are shown in Fig. 1. Both structures are composed of alternating layers of borohydride and ammonia borane. Upon incorporation of AB into the structure, the essential structural arrangements of BH_4^- anions and metal cations in the borohydride layers remain almost unchanged compared to the parent $LiBH_4$ and $Ca(BH_4)_2$ lattices (Figure S3 and S4). In the ammonia borane layers, the nearly square arrangement of NH_3BH_3 arrays is similar to the *bc*-plane arrangement of the ordered *Pmn21* phase of AB for LiBH · AB, or similar to the *ab*-plane lattice of AB for CaBH · AB. In LiBH · AB each Li^+ cation is tetrahedrally coordinated by three BH_4^- and one NH_3BH_3 with Li-B distances in the range of 2.535–2.631 Å. In CaBH · AB, each Ca^{2+} has octahedral coordination, surrounded by four BH_4^- and two NH_3BH_3 with Ca-B distances ranging from 2.899 Å to 2.923 Å. The distances between cations and the centers of surrounding ligands are consistent with those observed in the corresponding complex hydrides.[10,25–27] In LiBH · AB, the distances between the Li and the nearby hydridic H of NH_3BH_3 are 2.078 Å and 2.321 Å, comparable to those between Li and H in the BH_4^- (2.023–2.246 Å). The BH···HN distances between NH_3BH_3 and the adjacent BH_4^- are 2.248 Å to 2.254 Å, whereas the BH···HN separation between the neighboring NH_3BH_3's is 2.439 Å, longer than the van der Waals distance for the interaction constituting a dihydrogen bond (2.4 Å).[1] Therefore little dihydrogen bonding would be expected in the AB layers. Such a greatly weakened BH···HN interaction between NH_3BH_3 compared to the dihydrogen bond in the pristine AB (2.02 Å) is probably due to the strengthened interaction of NH_3BH_3 with Li^+ cations and with the adjacent H in the BH_4^-. As a result, the incorporation of AB into $LiBH_4$ crystal structure is primarily stabilized by their interactions with BH_4^- and Li^+. Different from LiBH · AB, the distance between BH···HN in the AB layers in CaBH · AB is 1.735 Å, significantly shorter than that in the pristine AB, indicating strong dihydrogen bonding in the AB layers. The NH_3BH_3 ligands also interact with nearby BH_4^- *via* dihydrogen bonding, as the BH···HN distances between NH_3BH_3 and the adjacent BH_4^- are 1.986 Å and 2.037 Å. Moreover, the distances between the Ca^{2+} and the nearby hydridic H of NH_3BH_3 are 2.441 Å and 2.504 Å, similar to those between the Ca^{2+} and H in the BH_4^- (2.412 Å to 2.477 Å). Consequently, unlike LiBH · AB, $Ca(BH_4)_2$ layers and AB layers are interwoven mainly by dihydrogen bonds throughout the CaBH · AB crystal structure.

The calculated B–N bond lengths in LiBH · AB and CaBH · AB are 1.596 Å and 1.591 Å, respectively, longer than those in $LiNH_2BH_3$ (1.547 Å) and $Ca(NH_2BH_3)_2$ (1.546 Å) but close to that in the solid NH_3BH_3 (~1.592 Å).[10] As previous calculations indicate, for metal amidoboranes, N attracts more electrons directly from the metals, which leads to a stronger bonding between B and N in the $NH_2BH_3^-$ ions.[10] In contrast, in borohydride ammonia borane, NH_3BH_3 stays in a molecular form and no electrons directly transfer from metal to N atom. Therefore, the nature of N–B would be similar to that in pure AB, leading to a comparable N–B bond length. Similarly, average H–N and H–B bond lengths are 1.030 Å and 1.222 Å in LiBH · AB and 1.032 Å and 1.222 Å in CaBH · AB, comparable to those in NH_3BH_3. These bond lengths indicate that no significant change occurs in the bonding nature of NH_3BH_3 during the formation of borohydride ammonia borane.

Neutron vibrational spectra were measured for LiBH · AB and CaBH · AB, which directly reflect the vibrational density of states and are particularly sensitive to the hydrogen vibrational modes (Fig. 2). The first-principles calculated NVS are also shown in Fig. 2. For CaBH · AB the observed phonon bands can be assigned to the rocking and librational modes of B–H in BH_4^- (30–40 meV, 50–60 meV), and of N–H and B–H in AB (42–45 meV; 90–98 meV); bending and deformation modes of B–H in BH_4^-(130–138 meV), and of N–H and B–H in AB (138–152 meV), and the N–B stretching mode in AB (101–103 meV). LiBH · AB shows a similar NV spectrum except for a relatively broad band in the range of 40–60 meV. The phonon modes in this range are from the collective rocking modes of B–H and N–H in BH_4^- and NH_3BH_3. In general, the calculated spectra agree reasonably well with the observed NV spectra for both compounds, and thus further support the validity of our determined structures. From the calculations, the B–H of BH_4^- and the B–H of AB stretching modes (285–300 meV) in LiBH · AB and CaBH · AB are within the same B–H stretching region of $LiBH_4$,[25] $Ca(BH_4)_2$,[28] and AB,[29] and the N–H stretching modes (400–417 meV) are also consistent with that of N–H in AB,[29] which suggests similar B–H and N–H bond lengths in the borohydride ammonia borane complex compared to the parent borohydrides and AB.

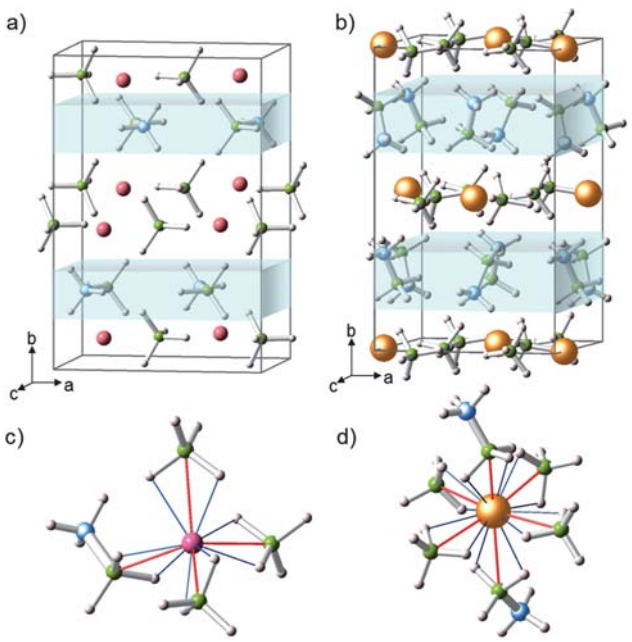

Fig. 1 (Top) Crystal structure of LiBH · AB and CaBH · AB. Li, Ca, B, N, and H atoms are represented by pink, orange, green, blue, and white spheres, respectively. The layers of AB are highlighted. (Bottom) Coordination environment of Li^+ and Ca^{2+} cations.

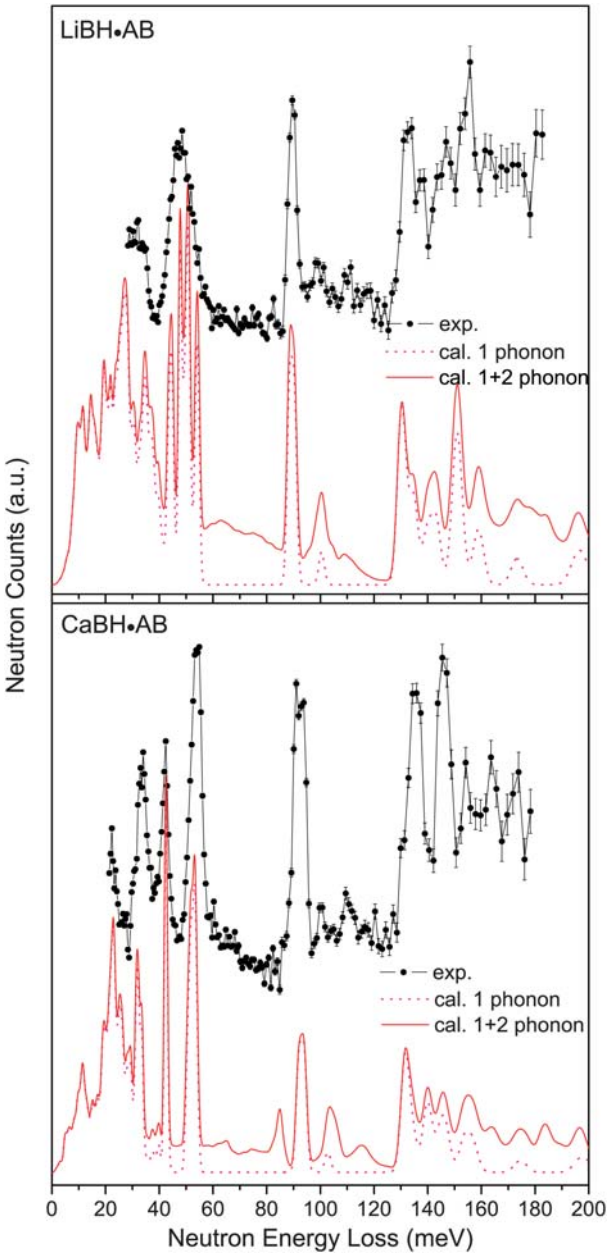

Fig. 2 Observed and calculated neutron vibrational spectra of LiBH · AB and CaBH · AB.

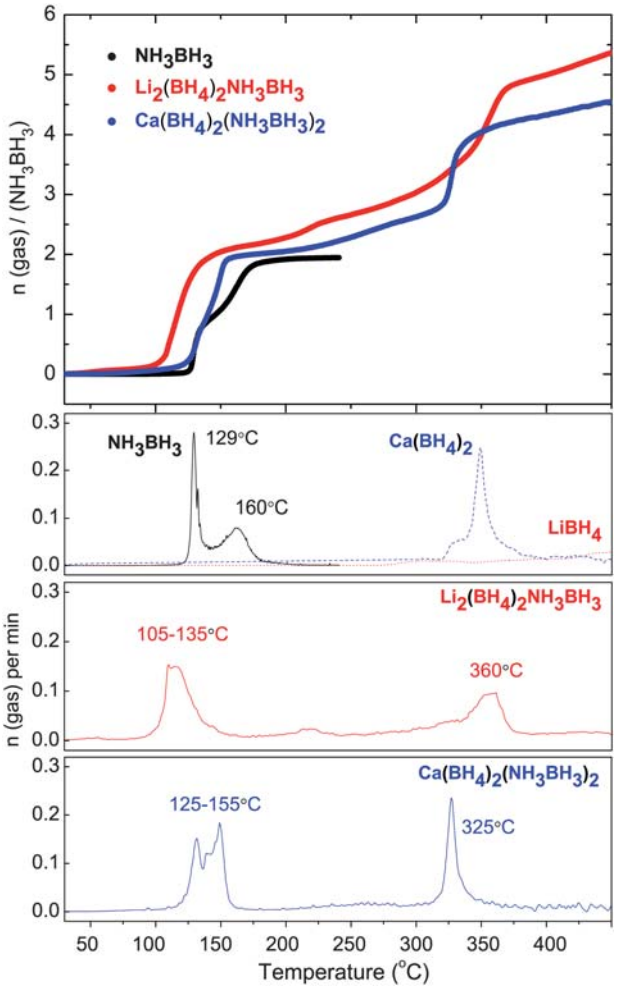

Fig. 3 TPD results of hydrogen release for LiBH · AB and CaBH · AB with 2 °C/min heating rate to 450 °C. Pure AB, $LiBH_4$ and $Ca(BH_4)_2$ were also measured for comparison. Note: H_2 just starts to release from $LiBH_4$ at 450 °C. The amount of hydrogen gas released (top panel) from LiBH · AB and CaBH · AB has been normalized as n (H_2 gas)/mol NH_3BH_3.

3.2 Hydrogen storage properties of $Li_2(BH_4)_2NH_3BH_3$ and $Ca(BH_4)_2(NH_3BH_3)_2$

Dehydrogenation of the LiBH · AB and CaBH · AB was investigated using temperature-programmed desorption (TPD) (Fig. 3). LiBH · AB decomposed initially at 105–135 °C with a further step occurring at 360 °C. The dehydrogenation of CaBH · AB resembles that of LiBH · AB, first at 125–155 °C and then at 325 °C. XRD patterns collected on LiBH · AB and CaBH · AB samples after the first desorption step show the formation of $LiBH_4$ and $Ca(BH_4)_2$, respectively (Fig. S5), suggesting that the first desorption step was mainly caused by the AB component. Pure AB releases 1.9 equivalents of H_2/mol AB at 129 °C and 160 °C under the same 2 °C/min heating rate, while the dehydrogenation temperatures of the AB component in LiBH · AB and CaBH · AB are lower than that of pure AB (Fig. 3). LiBH · AB and CaBH · AB can release a total of up to ~5.5 and ~4.5 equiv. of H_2, indicating that the second desorption process arises mainly from the borohydride components. Compared to pure $LiBH_4$ and $Ca(BH_4)_2$, the borohydride components in these complex compounds also release H_2 at slightly lower temperatures under the same heating rate (Fig. 3). After the complete desorption XRD showed only amorphous patterns for both compounds.

The quantitative gas desorption from LiBH · AB and CaBH · AB were characterized using a TGA-RGA (Fig. 4 and 5). The weight loss in the low temperature region is composed mainly of hydrogen, borazine and a small amount of diborane gases (Note: some ethylene gas was also observed, which might come from the 90% technical grade AB precursor). The high temperature weight loss appears to be primarily H_2 for both compounds. A breakdown of the contribution of each species to the weight loss is

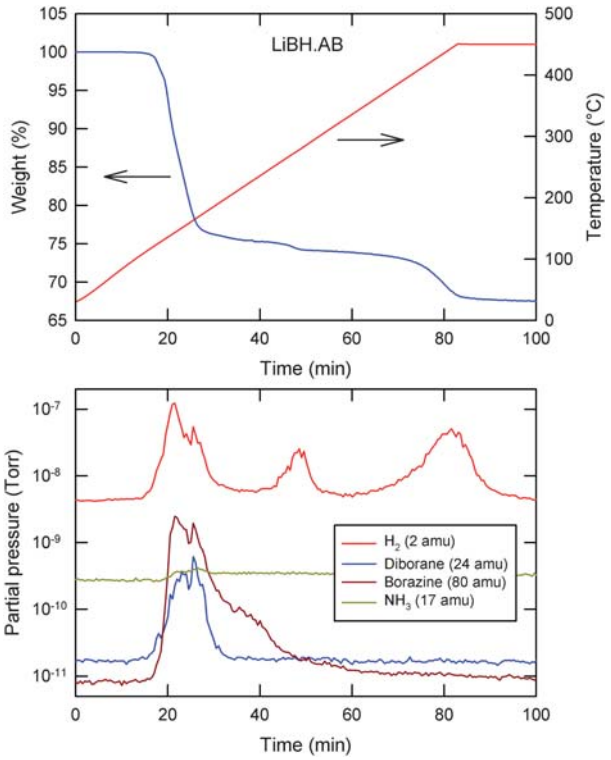

Fig. 4 TGA weight loss and the accompanying RGA partial pressures for LiBH · AB measured at 5 °C/min to 450 °C. Total mass results are summarized in Table 1.

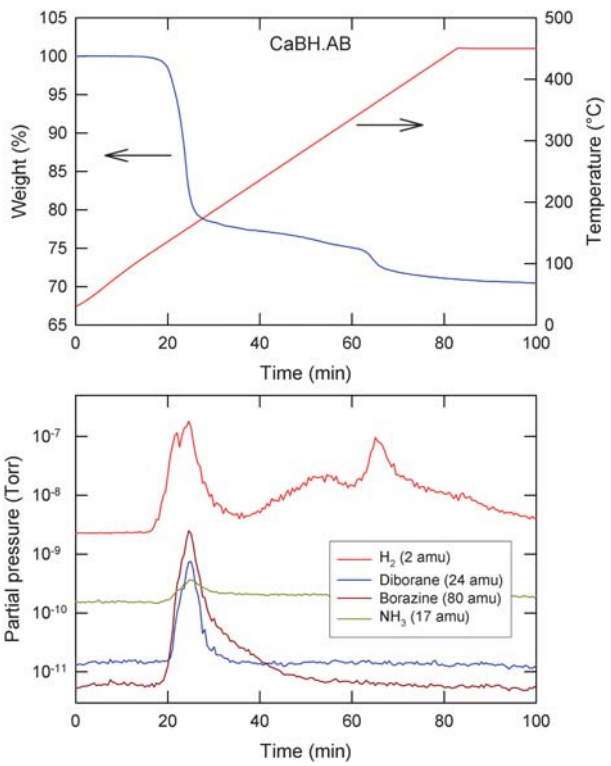

Fig. 5 TGA weight loss and the accompanying RGA partial pressures for CaBH · AB measured at 5 °C/min to 450 °C. Total mass results are summarized in Table 1.

Table 1 TGA weight loss in weight percent, and the corresponding gas species detected in the TGA exhaust. The mass spectrometer is calibrated for H_2, B_2H_6, and NH_3 gases; these are reported as mass fractions of the total evolved gas. The balance of the evolved gas is comprised of $(BH)_3(NH)_3$ and C_2H_4. $(BH)_3(NH)_3$ and C_2H_4 are not calibrated, and therefore mass fractions cannot be computed; for these gases comparisons to other gases are not valid, but comparisons can still be made within a column. A dash indicates that the species was not detected to within our instrumental resolution. All values are ± 20% relative

		RGA – calibrated			RGA – uncalibrated	
Sample	TGA weight loss (wt%)	H_2 Frac. (%)	B_2H_6 Frac. (%)	NH_3 Frac. (%)	$B_3N_3H_6$ (arb. units)	C_2H_4 (arb.)
LiBH.AB desorb 1	32.9	31	3.5	0.2	57	38
LiBH.AB desorb 2	2.4	100	—	—	—	—
CaBH.AB desorb 1	29.8	38	2.8	0.2	25	34
CaBH.AB desorb 2	2.9	100	—	—	—	—

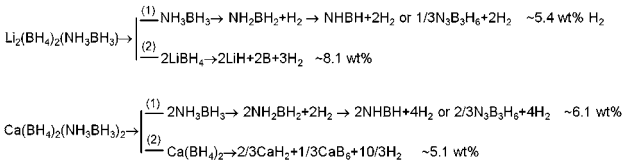

Scheme 1 Dehydrogenation Reactions of LiBH · AB and CaBH · AB.

shown in Table 1. From the MS patterns, the introduction of borohydride to the AB system can indeed suppress the release of ammonia, compared to ~25.3 wt% NH_3 in $Ca(NH_2BH_3)\cdot 2NH_3$,[13] and 2000 ppm NH_3 (or 1 equiv. H_2) in $LiNH_2BH_3$,[30] under the TPD measurement condition (*i.e.*, dynamic flow mode). Consistent with the XRD observations on the samples after the first desorption step, the contamination of borazine gas further confirms that during desorption, LiBH · AB and CaBH · AB first disproportionate into AB and borohydrides, and the AB component behaves similar to that of pristine AB, releasing both hydrogen and borazine gases.[31,32] With increasing temperature, the borohydride components in LiBH · AB and CaBH · AB further dehydrogenate and release 6.5 wt% and 5.1 wt% pure hydrogen, respectively. Therefore, the decomposition of LiBH · AB and CaBH · AB can be described by Scheme 1. From the TGA-MS analysis, the total hydrogen released from CaBH · AB is approximately 11.2 wt%, which agrees well with the calculated hydrogen loss (Scheme 1). While the observed total hydrogen released from LiBH · AB (*i.e.* 10.3 wt%) is less than the calculated the hydrogen loss, which is probably due to insufficient dehydrogenation and/or the more contamination from borazine and diborane.

Cycling properties of LiBH · AB and CaBH · AB were investigated by rehydrogenation of the desorbed samples at various stages. After dehydrogenation at 150 °C, LiBH · AB and CaBH · AB could not be rehydrogenated under 50 bar H_2, while pressurizing the samples at 300 °C under 50 bar H_2 after complete dehydrogenation shows about 1.5 wt% partial

absorption. Cycling capacities can be improved to 2.4 wt% under 82 bar H_2 at 400 °C (Fig. S6a and S6b). This indicates that the rehydrogenation originates primarily from the borohydride components. The XRD patterns of samples after hydrogenation show mainly the amorphous features except for the reflections of LiH and CaH_2 (Fig.S7 and S9). With limited information, we cannot tell whether the observed diffraction peaks are from the direct hydrogenation products or the recrystallization of the hydrides formed after dehydrogenation (Scheme 1).

The introduction of BH_4^- into NH_3BH_3 was assumed to deprotonate H^+ in the $-NH_3$ group of NH_3BH_3 and possibly form BH_3–NH_2–BH_3^-. However, in contrast to the formation of metal ammidoborane, where H^- in LiH and CaH_2 can easily attract H^+ in NH_3BH_3 and generate $NH_2BH_3^-$, no deprotonation was observed during the mixing of borohydrides and AB. Instead, AB molecules preferably interpenetrate into the borohydride framework, forming a layered borohydride ammonia borane complex. The interactions of the nearly charge neutral AB molecules with their surroundings are relatively weak compared to normal ionic or covalent compounds; therefore they can easily separate from the parent borohydrides during a thermal process. Also, unlike the recently reported $Ca(NH_2BH_3)\cdot NH_3$, where NH_3 molecules can be easily removed upon heating to form the deammoniation product of $Ca(NH_2BH_3)_2$, the decomposition nature of AB (*i.e.*, its propensity to decompose while melting) determines that it cannot be simply removed upon heating but rather desorbs H_2 as well as other toxic volatile gases.

It is noticeable that CaBH · AB produces much less borazine and diborane than LiBH · AB. This might be related to their structural details. As discussed above, CaBH · AB structures are stabilized by the strong intermolecular dihydrogen bonding in the AB layers, the dihydrogen bonding between AB and the surrounding BH_4^-, as well as by the interactions between AB and the Ca^{2+} throughout the crystal structure, whereas in LiBH · AB, the AB molecules mainly interact with the BH_4^- and Li^+. Thus, it is possible that in CaBH · AB, some H_2 releases before AB completely separates from the structure, and this consequently reduces the amount of borazine released. This implies that different metals, dopants and catalysts may be utilized to tune the dehydrogenation of these compounds. Investigations of other alkali and alkaline-earth borohydride ammonia borane compounds are now underway.

4 Conclusions

Two new high hydrogen content B-compounds, lithium borohydrides ammonia borane and calcium borohydrides ammonia borane, formulated as $Li_2(BH_4)_2NH_3BH_3$ and $Ca(BH_4)_2(NH_3BH_3)_2$, were successfully synthesized. Their crystal structures were determined using combined XRD and first-principles calculations. The high hydrogen contents of LiBH · AB (*ca.* 13.4 wt%) and CaBH · AB (*ca.* 11.2 wt%) render these compounds potential candidates for hydrogen storage. LiBH · AB and CaBH · AB can be partially hydrogenated with more than 2 wt% cycling capacities under 82 bar H_2 pressure at 400 °C. In addition, reduced NH_3 formation upon dehydrogenation was observed in borohydride ammonia borane compared to pure AB, metal ammidoborane, and amidoborane ammoniate. To minimize the borazine gas, further investigations in expanding the range of metals used in this class of compounds and the role of dopants or catalysts in controlling dehydrogenation are needed.

Acknowledgements

This work was partially supported by DOE through BES Grant No. DE-FG02-08ER46522 (G.S. and T. Y.) and EERE Grant No. DE-AI-01-05EE11104 (T. J. U.).

References

1 F. Stephens, V. Pons and R. T. Baker, *Dalton Trans.*, 2007, 2613–2626.
2 A. Gutowska, L. Li, Y. Shin, C. M. Wang, X. S. Li, J. C. Linehan, R. S. Smith, B. D. Kay, B. Schmid, W. Shaw, M. Gutowski and T. Autrey, *Angew. Chem., Int. Ed.*, 2005, **44**, 3578–3582.
3 F. H. Stephens, R. T. Baker, M. H. Matus, D. J. Grant and D. A. Dixon, *Angew. Chem., Int. Ed.*, 2007, **46**, 746–749.
4 M. E. Bluhm, M. G. Bradley, R. Butterick, U. Kusari and L. G. Sneddon, *J. Am. Chem. Soc.*, 2006, **128**, 7748–7749.
5 C. A. Jaska, K. Temple, A. J. Lough and I. Manners, *J. Am. Chem. Soc.*, 2003, **125**, 9424–9434.
6 M. C. Denney, V. Pons, T. J. Hebden, M. Heinekey and K. I. Goldberg, *J. Am. Chem. Soc.*, 2006, **128**, 12048–12049.
7 R. J. Keaton, J. M. Blacquiere and R. T. Baker, *J. Am. Chem. Soc.*, 2007, **129**, 1844–1845.
8 H. V. K. Diyabalanage, R. P. Shrestha, T. A. Semelsberger, B. L. Scott, M. E. Bowden, B. L. Davis and A. K. Burrell, *Angew. Chem., Int. Ed.*, 2007, **46**, 8995–8997.
9 Z. Xiong, C. K. Yong, G. Wu, P. Chen, W. Shaw, A. Karkamkar, T. Autrey, M. O. Jones, S. R. Johnson, P. P. Edwards and W. I. F. David, *Nat. Mater.*, 2008, **7**, 138–141.
10 H. Wu, W. Zhou and T. Yildirim, *J. Am. Chem. Soc.*, 2008, **130**, 14834–14839.
11 C. Wu, G. Wu, Z. Xiong, X. Han, H. Chu, T. He and P. Chen, *Chem. Mater.*, 2010, **22**, 3–5.
12 K. R. Graham, T. Kemmitt and M. E. Bowden, *Energy Environ. Sci.*, 2009, **2**, 706–710.
13 Y. S. Chua, G. Wu, Z. Xiong, T. He and P. Chen, *Chem. Mater.*, 2009, **21**, 4899–4904.
14 K. J. Fijalkowski and W. Grochala, *J. Mater. Chem.*, 2009, **19**, 2043–2050.
15 F. E. Pinkerton, G. P. Meisner, M. S. Meyer, M. P. Balogh and M. D. Kundrat, *J. Phys. Chem. B*, 2005, **109**, 6.
16 J. J. Vajo, S. L. Skeith and F. Mertens, *J. Phys. Chem. B*, 2005, **109**, 3719.
17 A. F. Gross, J. J. Vajo, S. L. Atta and G. L. Olsen, *J. Phys. Chem. C*, 2008, **112**, 5651–5657.
18 E. Ronnebro and E. H. Majzoub, *J. Phys. Chem. B*, 2007, **111**, 12045.
19 Certain commercial suppliers are identified in this paper to foster understanding. Such identification does not imply recommendation or endorsement by the NIST, nor does it imply that the materials or equipment identified are necessarily the best available for the purpose.
20 A. C. Larson, and R. B. Von Dreele, *General Structure Analysis System*, Report LAUR 86-748. Los Alamos National Laboratory, NM, 1994.
21 W. Zhou, H. Wu, M. R. Hartman and T. Yildirim, *J. Phys. Chem. C*, 2007, **111**, 16131.
22 P. Giannozzi, S. Baroni, N. Bonini, M. Calandra, R. Car, C. Cavazzoni, D. Ceresoli, G. L. Chiarotti, M. Cococcioni, I. Dabo, A. Dal Corso, S. Fabris, G. Fratesi, S. de Gironcoli, R. Gebauer, U. Gerstmann, C. Gougoussis, A. Kokalj, M. Lazzeri, L. Martin-Samos, N. Marzari, F. Mauri, R. Mazzarello, S. Paolini, A. Pasquarello, L. Paulatto, C. Sbraccia, S. Scandolo, G. Sclauzero, A. P. Seitsonen, A. Smogunov, P. Umari and R. M. Wentzcovitch, *J. Phys.: Condens. Matter*, 2009, **21**, 395502.
23 R. Car and M. Parrinello, *Phys. Rev. Lett.*, 1985, **55**, 2471.
24 G. Kresse, J. Furthmuller and J. Hafner, *Europhys. Lett.*, 1995, **32**, 729.

25 M. R. Hartman, J. J. Rush, T. J. Udovic, Jr, R. C. Bowman and S. J. Hwang, *J. Solid State Chem.*, 2007, **180**, 1298.
26 H. Wu, W. Zhou, T. J. Udovic, J. J. Rush and T. Yildirim, *Chem. Mater.*, 2008, **20**, 1245.
27 F. Buchter, Z. Lodziana, A. Remhof, O. Friedrichs, A. Borgschulte, Ph. Mauron, A. Züttel, D. Sheptyakov, G. Barkhordarian, R. Bormann, K. Chlopek, M. Fichtner, M. Sørby, M. Riktor, B. Hauback and S. Orimo, *J. Phys. Chem. B*, 2008, **112**(27), 8042–8048.
28 M. Fichtner, K. Chlopek, M. Longhini and H. Hagemann, *J. Phys. Chem. C*, 2008, **112**, 11575–11579.
29 N. J. Hess, M. E. Bowden, V. M. Parvanov, C. J. Mundy, S. M. Kathmann, G. K. Schenter and T. Autrey, *J. Chem. Phys.*, 2008, **128**, 034508.
30 T. Autrey. *PNNL Progress as Part of the Chemical Hydrogen Storage Center of Excellence*, DOE Hydrogen Annual Merit Review 2009 (http://www.hydrogen.energy.gov/pdfs/review09/st_18_autrey.pdf).
31 F. Baitalow, J. Baumann, G. Wolf, K. Jaenicke-Rossler and G. Leitner, *Thermochim. Acta*, 2002, **391**, 159–168.
32 G. Wolf, J. Baumann, F. Baitalow and F. P. Hoffmann, *Thermochim. Acta*, 2000, **343**, 19–25.

